PHASE RESETTING OF THE RHYTHMIC ACTIVITY OF EMBRYONIC HEART CELL AGGREGATES

Experiment and Theory

JOHN R. CLAY
Laboratory of Biophysics, Intramural Research Program, National Institute of Neurological and Communicative Disorders and Stroke, National Institutes of Health at the Marine Biological Laboratory, Woods Hole, Massachusetts 02543

MICHAEL R. GUEVARA AND ALVIN SHRIER
Department of Physiology, McGill University, Montreal, Quebec, Canada H3G 1Y6

ABSTRACT   Injection of a current pulse of brief duration into an aggregate of spontaneously beating chick embryonic heart cells resets the phase of the activity by either advancing or delaying the time of occurrence of the spontaneous beat subsequent to current injection. This effect depends upon the polarity, amplitude, and duration of the current pulse, as well as on the time of injection of the pulse. The transition from prolongation to shortening of the interbeat interval appears experimentally to be discontinuous for some stimulus conditions. These observations are analyzed by numerical investigation of a model of the ionic currents that underlie spontaneous activity in these preparations. The model consists of: I_x, which underlies the repolarization phase of the action potential, I_{K_2}, a time-dependent potassium ion pacemaker current, I_{bg}, a background or time-independent current, and I_{Na}, an inward sodium ion current that underlies the upstroke of the action potential. The steady state amplitude of the sum of these currents is an N-shaped function of potential. Slight shifts in the position of this current-voltage relation along the current axis can produce either one, two, or three intersections with the voltage axis. The number of these equilibrium points and the voltage dependence of I_{Na} contribute to apparent discontinuities of phase resetting. A current-voltage relation with three equilibrium points has a saddle point in the pacemaker voltage range. Certain combinations of current-pulse parameters and timing of injection can shift the state point near this saddle point and lead to an interbeat interval that is unbounded. Activation of I_{Na} is steeply voltage dependent. This results in apparently discontinuous phase resetting behavior for sufficiently large pulse amplitudes regardless of the number of equilibrium points. However, phase resetting is fundamentally a continuous function of the time of pulse injection for these conditions. These results demonstrate the ionic basis of phase resetting and provide a framework for topological analysis of this phenomenon in chick embryonic heart cell aggregates.

INTRODUCTION

Considerable interest has centered in recent years on the perturbing influences of brief duration electrical stimuli on the spontaneous rhythmic activity of nerve and cardiac cells (Perkel et al., 1964; Hartline, 1976; Ayers and Selverston, 1977; Winfree, 1977; Pinsker, 1977; Guttman et al., 1980; Ushiyama and Brooks, 1974; Jalife and Moe, 1976; Sano et al., 1978; Jalife and Antzelevitch, 1979, 1980; Jalife et al., 1980; Guevara et al., 1981). The reports on cardiac preparations have amplified the original observations of Weidmann (1951) concerning the effects of individual current pulses on the rhythmic behavior of spontaneously active cardiac Purkinje fibers. These experiments have several features in common. For example, a current pulse stimulus applied sometime after the occurrence of a cardiac action potential either advances or

potential event depending upon the polarity, the amplitude, and the duration of the pulse, and the time at which it was applied. In general, a depolarizing pulse of given amplitude and duration delays the time of occurrence of the next event when applied relatively early in the cycle, whereas it advances the time of the next event when applied later in the cycle. The effect is reversed for hyperpolarizing pulses. The transition point at which a depolarizing pulse produces neither a delay nor an advance moves to earlier times in the cycle as the amplitude of the pulse is increased. Moreover, the range of times of the delivery of the pulse for which the transition from delay to advance can be clearly discerned, narrows considerably as the pulse amplitude is increased. In fact, the transition is apparently discontinuous for sufficiently large pulse amplitudes or pulse durations (Jalife and Moe, 1976; Sano et al., 1978; Scott, 1979; Jalife et al., 1980; Guevara et al., 1981).

The above observations have prompted a number of theoretical investigations concerning the response of simple limit cycle oscillators to perturbations of brief duration (Scott, 1979; Winfree, 1980; Guevara and Glass, 1982; Guevara et al., 1983). Moreover, several authors have investigated phase resetting in ionic models of nerve and cardiac cell membranes (McAllister et al., 1975; Best, 1979; Guttman et al., 1980; DiFrancesco and Noble, 1982a; Guevara et al., 1982; Bristow and Clark, 1982; Guevara et al., 1983). However, in our view, there has not as yet appeared a detailed report describing the relationship between specific phenomena that occur during phase resetting and the underlying ionic currents, particularly with reference to the apparent discontinuity of phase resetting. We have attempted such a study using aggregates of cells derived with tissue culture techniques from the hearts of chick embryos. These preparations beat spontaneously and rhythmically under appropriate experimental conditions (see Methods). Aggregates are a suitable choice for this investigation even though they are multicellular preparations, because their small size, their spherical geometry, and the tight electrical coupling of cells within an aggregate lead to a virtually isopotential preparation (DeHaan and Fozzard, 1975; DeFelice and DeHaan, 1977; Clay et al., 1979; Clapham, 1979; Mathias et al., 1981). Several investigators have used this preparation for phase resetting studies (Scott, 1979; Guevara et al., 1981; Ypey et al., 1982). Moreover, the membrane currents underlying pacemaking in aggregates have recently been measured with the voltage clamp technique (Nathan and DeHaan, 1979; Shrier and Clay, 1980; Ebihara et al., 1980; Ebihara and Johnson, 1980; Clay and Shrier, 1981a, b; Shrier and Clay, 1982; Josephson and Sperelakis, 1982). Therefore, an analysis of phase resetting using these voltage clamp results for heart cell aggregates seems timely.

METHODS

Experimental

A full account of our experimental methods has been given elsewhere (Sachs and DeHaan, 1973; Clay et al., 1979; Clay and Shrier, 1981a). A brief account is as follows. Individual cells were dissociated at ambient temperature from the apical portions of the ventricles of 7-d old chick embryonic hearts using trypsin. The cells were transferred to a flask containing tissue culture medium (818A) having a potassium ion concentration of 1.3 mM. The flask was placed on a gyratory shaker for 48–96 h. During slow gyration cells aggregate into small spherical clusters 100–250 μm in diameter. The aggregates were transferred to a tissue culture dish containing culture medium for electrophysiological recording. The medium was gassed with a 5% CO_2, 10% O_2, and 85% N_2 gas mixture during gyration culture and during electrophysiological recordings. The temperature was maintained constant at 35° ± 0.5°C. Aggregate diameters were measured with an ocular reticle whose smallest division represented 18 μm. Measurements could be made to about half a division. Under these conditions aggregates beat spontaneously and rhythmically with a range of interbeat intervals (IBI) typically between 0.5 and 1 s. Intracellular recordings of spontaneous activity were made with glass microelectrodes filled with 3 M KCl. Current pulses were injected through the single voltage recording electrode. The amplitude of the pulse was measured with a virtual ground current-to-voltage converter.

Theoretical

Overview of Ionic Currents. Voltage clamp analysis of 7–d-old chick embryonic ventricular cells has revealed four ionic current components that contribute to the total membrane current throughout the range of membrane pacemaker potentials, -100 to -60 mV (Shrier and Clay, 1982). These components are (a) a time-dependent potassium ion current, I_{K_2}, with slow voltage-dependent kinetics having time constants of activation typically in the 0.1 to 1.0 s range; (b) a time-independent or background current, I_{bg}, which appears to be carried by a mixture of ionic species, most notably sodium, $I_{Na,b}$, and potassium, $I_{K,i}$; (c) a time-dependent current, I_K or I_x, which primarily determines the rate of repolarization; and (d) a sodium ion current, I_{Na}, with millisecond kinetics that primarily controls the maximal rate of rise of the upstroke of the action potential (V_{max}). The I_{K_2} component has also been reported for mammalian cardiac Purkinje fibers by Noble and Tsien (1968), although DiFrancesco (1981) and DiFrancesco and Noble (1982a) have recently reinterpreted this current in Purkinje fibers as an inward current, which they have termed I_f. DiFrancesco and Noble (1982b) have also suggested that the I_f model may provide an alternative representation for the Clay and Shrier (1981a, b) voltage clamp measurements. However, the pacemaker current kinetics in voltage-clamped aggregates near the potassium equilibrium potential, E_K, together with the developmental changes in pacemaker currents that occur after day 7 appear to require the original I_{K_2} rather than the I_f model (Clay and Shrier, 1981a, b; 1983). Moreover, the behavior of the reformulated model of cardiac Purkinje fiber in response to current pulse stimulation does not appear to be appreciably different from that of the earlier McAllister et al. (1975) model in which I_{K_2} is the pacemaker component (DiFrancesco and Noble, 1982a).

Mathematical Representaiton of Ionic Currents. Measurements of I_{K_2} for 7-d ventricular aggregates are given in Shrier and Clay (1980) and Clay and Shrier (1981a). The latter paper also contains a mathematical representation of the I_{K_2} results, which is given by

$$I_{K_2}(V, t) = s(V, t) \cdot I^o_{K_2} \cdot f_{K_2}(V), \tag{1}$$

where V is the membrane potential and the activation parameter, s, is governed by the equation

$$ds(V, t)/dt = -[\alpha_s(V) + \beta_s(V)] \cdot s(V, t) + \alpha_s(V), \tag{2}$$

where the rate constants, α_s and β_s, are given (in inverse seconds) by

$$\alpha_s(V) = \alpha^o_s \cdot (V + E_2)/\{1 - \exp[-\alpha^1_s \cdot (V + E_2)]\} \tag{3}$$

$$\beta_s(V) = \beta^o_s \cdot \exp[-\beta^1_s \cdot (V + E_2)]. \tag{4}$$

$I^o_{K_2}$ is a constant and

$$f_{K_2}(V) = x^2 \cdot (p_+ - p_-)/(1 + x + x^2), \tag{5}$$

with

$$x = p_-/p_+, \tag{6}$$

$$p_+ = 1/\{1 + \exp[q(V - E_K)/kT]\}, \tag{7}$$

and

$$p_- = 1 - p_+. \qquad (8)$$

The values of the various parameters in the above expressions that describe the typical results in Clay and Shrier (1981a) are $\alpha_s^o = 1.05 \text{ s}^{-1}$, $\beta_s^o = 0.095 \text{ s}^{-1}$, $\alpha_s^1 = 0.2 \text{ mV}^{-1}$, $\beta_s^1 = 0.075 \text{ mV}^{-1}$, $E_2 = -58 \text{ mV}$, $I_{K_2}^o = 545$ nA, and the potassium equilibrium potential, $E_K = -124 \text{ mV}$. The constants q, k, and T in Eq. 7 are, respectively, the unit electronic charge, the Boltzmann constant, and the absolute temperature. At $T = 35°C$, $kT/q = 26.6 \text{ mV}$. We have used $kT/q = 25 \text{ mV}$ throughout this study. The amplitude of $I_{K_2}^o$ and all other currents given below have been scaled for a 200 μm diam (D) aggregate using the observation of Clay et al. (1979) that the electrical parameters of aggregates of different sizes scale according to D^3.

The motivation for the above expressions is that time-dependent change in current following voltage clamp steps in the pacemaker voltage range follows a single exponential time course. Hence, we have represented the time dependence of I_{K_2} by a single parameter, s, which obeys first-order kinetics. The time constant $\tau_s(V) = (\alpha_s[V] + \beta_s[V])^{-1}$ is, therefore, a direct experimental observation. The voltage dependence of τ_s describes a bell-shaped curve having a maximum value of ~1 s at $v \simeq -80 \text{ mV}$, and smaller values either above or below -80 mV. For example, $\tau_s \simeq 0.5 \text{ s}$ for $V = -100 \text{ mV}$ and $\tau_s \simeq 0.2 \text{ s}$ for $V = -60 \text{ mV}$. The steady state value of the variable for activation of I_{K_2}, $s_\infty = \alpha_s(V)/(\alpha_s[V] + \beta_s[V])$, is also directly measured from the amplitude of the tail currents following return of the voltage to holding potential (Clay and Shrier, 1981a). These measurements for τ_s and s_∞ were fitted with the forms of $\alpha_s(V)$ and $\beta_s(V)$ given in Eqs. 3 and 4, which are similar to those used by Hodgkin and Huxley (1952) to empirically describe their voltage clamp measurements of potassium current in squid giant axons. The fully activated current, $I_{K_2}^o \cdot f_{K_2}(V)$, i.e., the pacemaker current that flows across the membrane when $s = 1$, is also determined experimentally, using the ratio of the time-dependent current during a clamp step to the time-dependent (tail) current following return to holding potential (Noble and Tsien, 1968; Clay and Shrier, 1981a). The specific functional form for $f_{K_2}(V)$ in Eq. 5 is motivated by the widely accepted view of the ion permeation process in biological membranes. Ions are believed to move in single file through narrow pores or channels widely spaced throughout the membrane. Each channel is guarded by a gate molecule that is either open, thereby allowing ion flow, or closed, thereby preventing ion flow. The s parameter in Eqs. 1 and 2 describes this gating process for I_{K_2} channels. That is, s can be viewed either as the probability that any single channel is open or as the fraction of open I_{K_2} channels throughout an aggregate. The $f_{K_2}(V)$ term in Eq. 5 can be viewed as describing the voltage dependence of current flow through an open channel. If the channel is ohmic, $f_{K_2}(V)$ is simply proportional to $(V - E_K)$, the driving force. However, potassium channels in muscle membranes are, in general, nonohmic. They allow current to flow more readily in the inward than the outward direction, a process that is termed inward rectification (Katz, 1949). The I_{K_2} channels in the aggregate are strong inward rectifiers when the external potassium concentration is 1.3 mM. That is, $f_{K_2}(V)$ reaches a maximal outward value 15-20 mV positive to E_K. It declines toward zero at more positive potentials nearly reaching a zero value for $V \geq -50$ mV. Consequently, $f_{K_2}(V)$ has a negative slope throughout the pacemaker potential range. This process is modeled in Eq. 5 by a two site, single file channel with a membrane bound blocking particle that is kept out of the channel by inward current flow and is knocked into the channel by outward current flow (Clay and Shlesinger, 1977, 1983; Clay and Shrier, 1981a).

The background current, I_{bg}, is determined in Clay and Shrier (1981a) by subtracting the steady state value of I_{K_2}, I_{K_2} (V, $t \rightarrow \infty$) $= s_\infty I_{K_2}^o$ $f_{K_2}(V)$, from the total current. That is, I_{bg} consists of nongated channels, channels that are open at all potentials. This component also displays inward rectification. Moreover, because its reversal potential, -40 mV, does not correspond to the Nernst equilibrium potential of any of the ionic

species that permeate the membrane, it appears to be a mixture of inward and outward current components. Consequently, I_{bg} is modeled in Clay and Shrier (1981a) by two components, an inwardly rectifying, outward current, I_{K_1}, carried primarily by potassium ions and an ohmic, inward current, $I_{Na,b}$, carried by sodium ions. That is,

$$I_{bg} = I_{K_1} + G_{Na,b} \cdot (V - E_{Na}). \qquad (9)$$

This expression was fitted to the I_{bg} experimental results using

$$I_{K_1} = I_{K_1}^o y^4 \cdot (p_+^1 - p_-^1)/(1 + y + y^2 + y^3 + \gamma \cdot y^4)$$
$$+ G_{K_1}^o (V - E_1)/\{1 - \exp[-q(V - E_1)/kT]\}, \qquad (10)$$

where

$$y = p_-^1/p_+^1, \qquad (11)$$

$$p_+^1 = 1/\{1 + \exp[q(V - E_3)/kT]\}, \qquad (12)$$

$$p_-^1 = 1 - p_+^1. \qquad (13)$$

The left-hand term in Eq. 10 is similar to $f_{K_2}(V)$ in Eq. 5, except that it corresponds to a channel with four ion-selective sites rather than two. This form for I_{K_1} was used because the range of potentials over which rectification occurs for I_{K_1} is narrower than the range of rectification of I_{K_2} (Clay and Shrier, 1981a). The I_{K_1} results further differ from I_{K_2} in that they exhibit a secondary increase of outward current for $V \gg E_K$. This effect is modeled by the second term in Eq. 10, whose functional form was taken directly from the model of I_{K_1} in cardiac Purkinje fibers of McAllister et al. (1975). The values of the various parameters in Eqs. 9–13 that provide a fair representation of the typical results in Clay and Shrier (1981a) are $I_{K_1}^o = 220 \text{ nA}$, $G_{Na,b} = 0.215 \mu S$, $E_{Na} = 40 \text{ mV}$, $\gamma = 0.58$, $G_{K_1}^o = 1.2 \mu S$, $E_1 = -40 \text{ mV}$, and $E_3 = -90 \text{ mV}$.

The I_x component is a time-dependent channel that is activated at $V \geq -50 \text{ mV}$. It decays to zero in the pacemaker range of potentials. The current-voltage relation of the I_x channel is approximately independent of voltage for $-90 \leq V \leq -55 \text{ mV}$ and its kinetics are described by a single parameter, s_x, having first-order kinetics. Its time constant, τ_x, as a function of potential, is described by a bell-shaped curve having a maximal value of approximately 3 s at $V = -35 \text{ mV}$. In the pacemaker range of potentials, τ_x is much less than τ_s (Clay and Shrier, 1981a; Shrier and Clay, 1982; J. R. Clay and A. Shrier, unpublished results). We have modeled these results with

$$I_x = I_x^o \cdot s_x (V, t), \qquad (14)$$

with

$$ds_x(V, t)/dt = -[\alpha_x(V) + \beta_x(V)] \cdot s_x(V, t) + \alpha_x(V), \qquad (15)$$

where

$$\alpha_x(V) = \alpha_x^o \cdot (V + E_x)/\{1 - \exp[-\alpha_x^1 \cdot (V + E_x)]\}, \qquad (16)$$

$$\beta_x(V) = \beta_x^o \cdot \exp[-\beta_x^1 \cdot (V + E_x)], \qquad (17)$$

with $I_x^o = 75 \text{ nA}$, $\alpha_x^o = 0.04 \text{ s}^{-1}$, $\beta_x^o = 0.01 \text{ s}^{-1}$, $\alpha_x^1 = 0.1 \text{ mV}^{-1}$, $\beta_x^1 = 0.1 \text{ mV}^{-1}$, and $E_x = -10 \text{ mV}$. We note that this is a preliminary model of I_x, which undoubtedly will undergo revision when further experimental results have been obtained. However, Eqs. 14–17 provide an adequate representation of I_x in the -90 to -55 mV range of potentials at an external potassium concentration of 1.3 mM.

The I_{Na} component has been measured in embryonic heart cells by Ebihara et al. (1980) and Ebihara and Johnson (1980). We have used the mathematical formulation of these results given by the latter authors

$$I_{Na} = G_{Na} \cdot m^3(V, t) \cdot h(V, t) \cdot (V - E_{Na}), \qquad (18)$$

where

$$dm(V, t)/dt = -[\alpha_m(V) + \beta_m(V)] \cdot m(V, t) + \alpha_m(V), \quad (19)$$

$$dh(V, t)/dt = -[\alpha_h(V) + \beta_h(V)] \cdot h(V, t) + \alpha_h(V), \quad (20)$$

with rate constants (in inverse seconds) given by

$$\alpha_m(V) = -320(V + 47.13)/\{\exp[-0.1(V + 47.13)] - 1\} \quad (21)$$

$$\beta_m(V) = 80 \exp(-V/11) \quad (22)$$

$$\alpha_h(V) = 135 \exp[-(V + 80)/6.8] \quad (23)$$

$$\beta_h(V) = 3.56 \cdot 10^3 \exp(0.079 \cdot V)$$
$$+ 3.1 \cdot 10^8 \exp(0.35 \cdot V) \quad (24)$$

and $G_{Na} = 500~\mu S$, $E_{Na} = 40$ mV. Ebihara et al. (1980) and Ebihara and Johnson (1980) measured I_{Na} from 11-d-old heart cell aggregates. We have assumed that their results are also appropriate for 7-d-old hearts based on the observation that V_{max} of the action potential appears to be the same at both stages (Clay and Shrier, 1981b).

The above expressions for I_{K_2}, I_{bg}, I_x, and I_{Na} comprise what we hereafter term Model I (Results). Model II is the same as Model I except for two changes in the background current: $G_{Na,b} = 0.16~\mu S$ and $G_{K_1}^o = 0.9~\mu S$, rather than $G_{Na,b} = 0.215~\mu S$ and $G_{K_1}^o = 1.2~\mu S$.

Computer Simulations of Pacemaker Voltage Changes. The membrane potential, V, was determined from the ionic currents in the standard way, by numerically integrating the equation

$$dV/dt = -(I_{ionic} + I_{stim})/C_i, \quad (25)$$

where $I_{ionic} = I_{K_2} + I_{bg} + I_x + I_{Na}$, I_{stim} is the externally applied current and C_i is the input capacitance of an aggregate. We have used $C_i = 0.023~\mu F$, which is appropriate for a 200 μm diam aggregate (Clay et al., 1979). The initial conditions, which we used for all simulations, were $V = -70$ mV, $s = 1$, $s_x = 1$, $m = 0$, and $h = 1$. These values approximate the state of the I_{K_2}, I_x, and I_{Na} gating parameters before the later phase of repolarization. We assume that I_{K_2} and I_x are fully activated by the end of the plateau phase of the action potential, and that s and s_x remain essentially unchanged during repolarization before the time at which $V = -70$ mV.

The initial starting time for all simulations was chosen to be $t = 150$ ms, which roughly corresponds to the duration of the action potential preceding $V = -70$ mV on the repolarization phase. Eq. 25 was integrated in double precision using an Euler fixed-step implementation of the Rush and Larsen (1978) algorithm to determine the potential change subsequent to $t = 150$ ms. An integration time step of 50 μs was used for most of our simulations. A smaller step (as small as 1 μs) was used to investigate the critical region of the phase resetting curve (Results). A current pulse of 20-ms duration was applied at various points in the unperturbed pacemaker cycle. The simulations were stopped when the potential reached the threshold of the action potential, which was arbitrarily chosen to be $V = -55$ mV.

RESULTS

Current-Voltage Relations (IV)

The respective contributions of the various ionic currents (Methods) to the total membrane pacemaker current are illustrated by curves a–e in Fig. 1. Curve a, which is the same for both Model I and II, represents the sum of the fully activated I_{K_2} component and the steady state amplitude of I_{Na}, i.e., $I_{K_2}^o \cdot f_{K_2}(V) + G_{Na}~m_\infty^3 h_\infty \cdot (V - E_{Na})$.

Curve b represents $I_{K_2}^o \cdot f_{K_2}(V) + I_{bg}(V) + G_{Na}~m_\infty^3 h_\infty \cdot (V - E_{Na})$. Curve c represents the total steady state current-voltage relation (IV), i.e., $s_\infty I_{K_2}^o \cdot f_{K_2}(V) + I_{bg}(V) + G_{Na}m_\infty^3 h_\infty \cdot (V - E_{Na})$. Curve d represents $I_{bg}(V) + G_{Na} \cdot m_\infty^3 h_\infty \cdot (V - E_{Na})$. The difference between c and d, therefore, is the steady state amplitude of I_{K_2}. Curve e represents the steady state IV in the absence of I_{Na}, i.e., $s_\infty I_{K_2}^o \cdot f_{K_2}(V) + I_{bg}(V)$. (The I_x component is not shown in Fig. 1, since the steady state amplitude of I_x is virtually nil for pacemaker potentials.) The term steady state in this context refers to the measurement of membrane current either in constant voltage clamp conditions ($t \to \infty$), or at the end of a voltage clamp pulse having a duration significantly greater than the time constants of all of the gated ionic channels that contribute to the total current. Curve e in Model I and II is to be compared with the experimental IV in Fig. 2 of Clay and Shrier (1981a) from an aggregate in tissue culture medium containing 1.3 mm K_o and tetrodotoxin (TTX), an agent that blocks both I_{Na} and spontaneous activity. Curves e of both Models I and II lie well within the range of the IV's that were experimentally observed. A further comparison between theory and experiment can be made with regard to the resting potential (E_r) of aggregates in TTX conditions. Experimentally, E_r is approximately -60 mV ($E_r = -56 \pm 7$ mV, mean $\pm$ SD, $n = 11$, Clay and Shrier, 1981a; $E_r = -57 \pm 10$ mV, mean $\pm$ SD, $n = 12$, Colizza et al., 1983). The E_r of curve e in Model I is -63.4 mV, which is consistent with these observations. The E_r of Model II is -71.8 mV. Some aggregates rest as negatively as -70 to -75 mV, although this range of E_r was somewhat atypical for 1.3 mm K_o (Clay and Shrier, 1981a). The addition of I_{Na} to curve e in Model I removes the equilibrium point in the pacemaker region, whereas the addition of I_{Na} to curve e in Model II shifts the equilibrium point slightly in the positive direction to -70.8 mV. It also introduces a second intersection of the IV with the voltage axis at $V = -66.7$ mV (inset of Fig. 1 B). That is, I_{Na} contributes an inward current to the steady state IV in the range of pacemaker potentials positive to -70 mV. The underlying mechanism of this current is a slight overlap between the activation curve of the I_{Na} channel, m_∞, and the inactivation curve, h_∞. This so-called "window current" (Attwell et al., 1979) contributes to the region of negative slope in the steady state IV, because $m_\infty^3 h_\infty$ is an increasing function of potential in the pacemaker voltage range and the driving force for sodium ions ($V - E_{Na}$; $E_{Na} = +40$ mV) is inward for potentials in the pacemaker range. Consequently, the total current is a single-humped function of potential for $-90 \leq V \leq -55$ mV that makes possible the existence of either no zero-current crossings of the IV (equilibrium points) in the pacemaker voltage range (Model I) or two such equilibrium points (Model II, inset of Fig. 1 B). The IV could also just touch the voltage axis, thereby giving one equilibrium point (bifurcation condition). There is also an additional zero crossing in both models at $V \simeq -25$ mV, which is not

shown in Fig. 1. The difference between Model I and II concerning the number of equilibrium points is of critical significance for our final conclusion (Discussion).

Phase Resetting of Model I

Experimental records of phase resetting are shown in the left-hand panel of Fig. 2 for an aggregate having an unperturbed interbeat interval (IBI_0) of ~0.5 s, which is near the lower end of the experimental range of IBI_0. The qualitative features of the dynamics displayed by this aggregate in response to depolarizing pulses were similar to those of 18 other preparations with values of IBI_0 ranging from 450 to 950 ms. In 10 of these preparations at least 5 different levels of current stimulus were used. Current pulses of 20-ms duration were applied at various times (t_{stim}) in the unperturbed cycle, as indicated by the stimulus artifact. The amplitude of the pulse was 5 nA for the records in row A; 8 nA for the records in row B. The initial time, $t_{stim} = 0$, was arbitrarily chosen to correspond to 0 mV on the upstroke of the action potential. When the pulse was applied near to the time of occurrence of the maximum diastolic potential (MDP), the time of occurrence of the succeeding action potential (IBI) was delayed slightly in both row A and B. As t_{stim} was increased, IBI increased in a gradual, continuous manner for the lower amplitude stimulus (row A), and then decreased continuously to values below IBI_0. The results for the higher amplitude stimulus (row B) exhibit an abrupt transition from maximum prolongation to maximum shortening of IBI at t_{stim} ~ 170 ms.
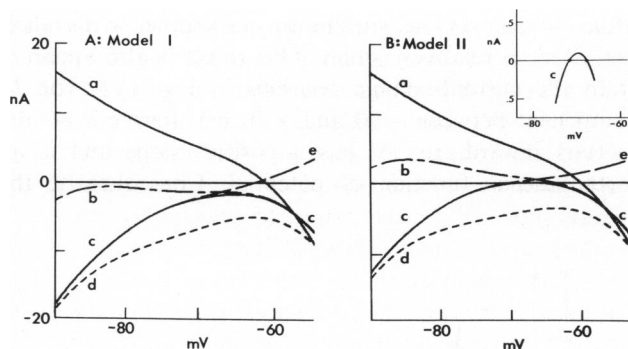

FIGURE 1   Current-voltage relations (IV); A: Model I; B: Model II. (a) Steady state amplitude of the sum of I_{Na} and I_{K_2} with $s = 1$ at all potentials. This curve is the same for both Model I and Model II. (b) Steady state of the sum of I_{Na}, I_{bg}, and I_{K_2} with $s = 1$. This curve differs from Models I and II because of the different parameters used for I_{bg} (Methods). (c) Total steady state IV, that is, $I_{Na} + I_{K_2} + I_{bg}$, with s at its appropriate steady state value for each potential. (d) Steady state amplitude of $I_{bg} + I_{Na}$. The difference between curves c and d represents the steady state amplitude of I_{K_2}. (e) Steady state IV in the absence of I_{Na}, i.e., $I_{K_2} + I_{bg}$, with s at its appropriate steady state value for each potential. This curve corresponds to aggregates treated with TTX (Results). Inset of panel B: Curve c of Model II with the current axis expanded to illustrate the equilibrium points at $V_1 = -70.8$ mV and $V_2 = -66.7$ mV. In both Models I and II there is a third equilibrium point at $V_3 \simeq -25$ mV.
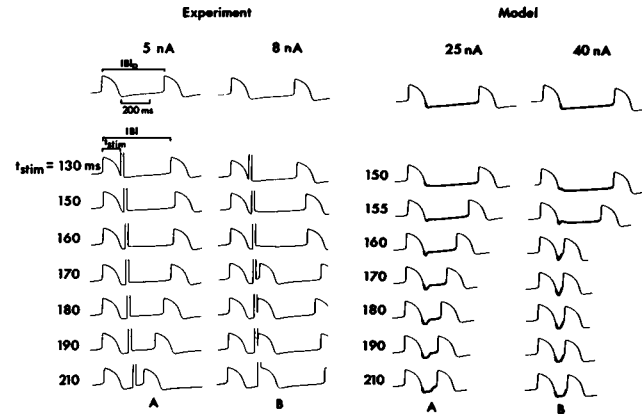

FIGURE 2   Phase resetting for a preparation with $IBI \simeq 0.5$ s. Left-hand panels: experimental recordings from a preparation having a diameter of 114 μm and an IBI_0 of 0.44 s. A depolarizing pulse of 20-ms duration and either 5 nA (row A) or 8 nA (row B) amplitude was applied starting at the times indicated to the left of row A. The MDP of the control is -88 mV, maximum overshoot potential is $+25$ mV. The perturbed interbeat interval (IBI) is defined as the time from 0 mV on the upstroke phase of the action potential preceding current injection to the corresponding time of the 0 mV crossing of the action potential subsequent to the pulse. Right-hand panels: simulations of phase resetting in Model I for a 20-ms pulse of 25-nA (row A) or 40-nA (row B) amplitude applied at the times indicated to the left of row A. The action potentials (thinner solid lines) are experimental recordings that were grafted onto the simulation curves (thicker solid lines).

Simulations using Model I, which is appropriate for an IBI_0 of $\simeq 0.5$ s, are shown in the right-hand panel of Fig. 2. The unperturbed model pacemaker is shown above both phase resetting panels. In all of these records the thick solid lines correspond to the computer simulations. The action potentials in these records are experimental records that were grafted onto the numerically simulated curves. This procedure is necessary, since we have at present only a partial model of voltage changes in aggregates that covers only the pacemaker range of potentials. Nevertheless, the model provides a faithful representation of the unperturbed pacemaker and can be used to investigate phase resetting for pacemaker potentials. The unperturbed model rapidly hyperpolarizes from $V = -70$ mV, which is the initial condition, to an MDP of -93 mV, followed by a gradual, nearly linear pacemaker depolarization to threshold. The current pulse stimulus produces a slight increase of IBI when it is applied close to MDP. It also reduces IBI, as t_{stim} is increased, in a gradual way for a small pulse (row A) and in an apparently discontinuous way for a larger pulse (row B), in a manner similar to that observed experimentally. However, there are some apparent quantitative discrepancies between the experiment and the model. For example, the smaller pulse amplitude in the model is 25 nA and the larger pulse is 40 nA, as compared with 5 and 8 nA in the experimental recordings. This is because the model is formulated assuming an aggregate diameter (D) of 200 μm. The preparation of Fig. 2 had a diameter of 114 μm. Since the membrane area of an aggregate scales

with D^3 (Clay et al., 1979), the model currents of 25 nA and 40 nA for a 200 μm diam aggregate actually correspond to currents of 4.6 and 7.4 nA, respectively, for a 114 μm diam aggregate. However, the maximum prolongation of IBI in the model for the 40 nA pulse is only 3% greater than IBI_0, whereas the experimental value of IBI has a maximal value that is 25% greater than IBI_0 for the 8 nA pulse amplitude. The model does successfully mimic the transition from a continuous to an apparently discontinuous IBI vs. t_{stim} relation as the pulse amplitude is increased. This point is further illustrated by the normalized phase resetting curves shown in Fig. 3 both for the experiment of Fig. 2 and for Model I. The experimental results in panel A of Fig. 3 also illustrate that there is only a small effect on IBI of a 5–8-nA current pulse applied during the plateau phase of the action potential. The calculations in panel B of Fig. 3 illustrate phase resetting on a finer time scale than was used in Fig. 2 or Fig. 3 A. Increments in t_{stim} of 0.5 ms were used for both the 25 nA (curve a) and the 40 nA simulations (curve b), except for the critical region of curve b for which 10-μs increments were used. The points merge together to give the appearance of a continuous, solid line for curve a. Curve b is also continuous, although the continuity is apparent only when 10 μs or smaller increments in t_{stim} are used in the critical region ($t_{stim} \simeq 158$ ms). Thus, Model I has resetting behavior that is continuous at each of the two current-pulse amplitudes. It is difficult, if not impossible, to say whether or not the experimental response at higher than 8 nA is continuous (Discussion).

The model results in Figs. 2 and 3 are further amplified by the current-voltage trajectories shown in Fig. 4. These curves were obtained by plotting the total membrane ionic current, $I_{K_2} + I_{bg} + I_{Na} + I_x$, as a function of membrane potential. The solid line that surrounds all of the other curves in both Fig. 4 A and B represents the unperturbed trajectory. This trajectory is part of the complete current-voltage cycle during spontaneous activity. The slight bend

of the curve near -60 mV represents the initial increase of I_{Na} associated with the fast upstroke phase of the action potential. To represent this part of the cycle, the trajectory would be continued to current-voltage phase coordinates of $I \simeq -3,000$ nA and $V \simeq -20$ mV corresponding to $V_{max} \simeq 150$ V/s. The phase point would then return to $I = 0$ at $V \simeq +30$ mV, which is the maximal overshoot potential. It would then move upwards and to the left, reaching a maximum outward current of about 80 nA at approximately -60 mV, which corresponds to V_{max} on the repolarization phase. The initial point of our simulations ($V = -70$ mV) is close to this V_{max} phase point during repolarization. The other lines in Fig. 4 correspond to trajectories during current-pulse perturbations (dotted lines) and after termination of the current pulses (solid lines). These results demonstrate that the paths followed by the trajectories are qualitatively similar for both the 25- and 40-nA pulse amplitudes.

Relationship of Normal Pacemaking to Ionic Currents in Model I

The individual contributions of I_x, I_{Na}, I_{bg}, and I_{K_2} to the evolution of the membrane voltage during unperturbed activity (Figs. 2 and 4) are illustrated in Fig. 5 A. The initial hyperpolarizing phase of the control simulation from -70 to -93 mV is mainly due to the outward I_x current (top panel of Fig. 5 A). The middle panel of Fig. 6 shows that τ_x is very small during this phase. The first part of pacemaker depolarization from 160 to 350 ms is associated with changes in I_{K_2} and I_{bg}, with little change in either I_x or I_{Na}. The sum of the former pair of components is inward, although they very nearly balance one another so that their net effect is relatively small. This result is also apparent from the current-voltage relations in Fig. 1 A. The I_{bg} component between -90 and -70 mV (curve d of Fig. 1 A) is inward. Its IV has a positive slope and is an instantaneous function of potential. Consequently, the
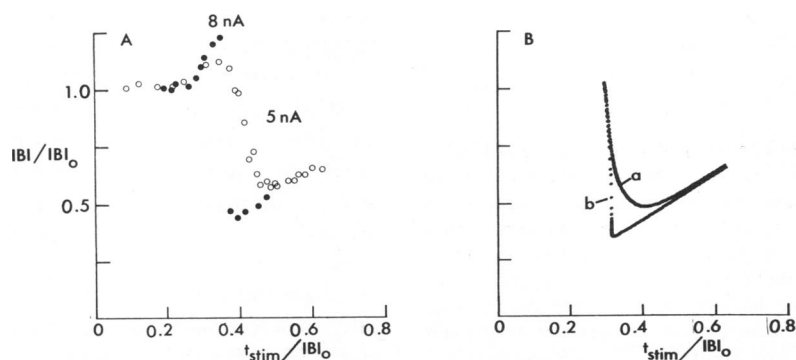

FIGURE 3 Phase resetting curves corresponding to the results of Fig. 2. Left-hand panel: normalized interbeat interval (IBI/IBI_0) as a function of the relative time in the unperturbed cycle of stimulus injection (t_{stim}/IBI_0) for the experimental results of Fig. 2. Pulse amplitude was either 5 nA (o) or 8 nA (●). Right-hand panel: phase resetting of Model I for (a) 25-nA or (b) 40-nA pulses. The increment is t_{stim} for curve a was 0.5 ms. These results merge to give the appearance of a continuous curve. The increment in t_{stim} for curves b was also 0.5 ms, except in the critical region for which an increment of 10 μs was used.
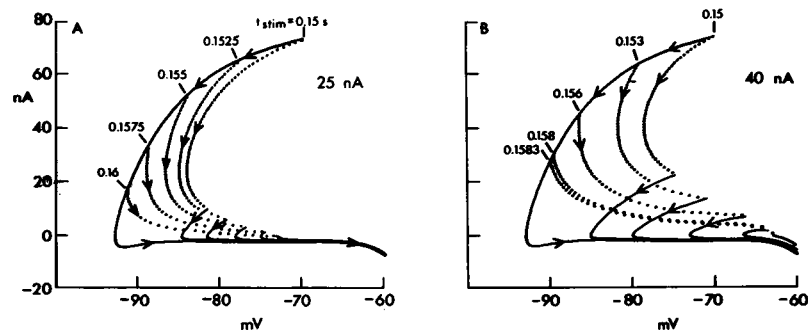
FIGURE 4 Current-voltage trajectories for Model I. Left-hand panel: 25-nA current pulses. Right-hand panel: 40-nA current pulses. The outermost solid curve in both panels corresponds to the unperturbed trajectory, as described in the text. The time of initiation of each pulse is indicated alongside the unperturbed trajectory. The dotted lines ($\cdots$) show the trajectory during current injection. The solid line (——) beginning at the end of each of the dotted lines corresponds to the trajectory following termination of current injection. The arrows show the direction of increasing time.

amplitude of I_{bg} at any given time can be read directly from its IV curve. At -70 mV, it is relatively small, and at -93 mV it is relatively large. Therefore, its magnitude rapidly increases during the initial phase of the simulation (Fig. 5 A), because the membrane potential rapidly hyperpolarizes toward MDP. It subsequently diminishes in amplitude during the pacemaker phase, as the potential slowly depolarizes toward threshold. The amplitude of I_{K_2} usually cannot be read directly from its IV curve, because it is not an instantaneous function of potential. The activation of I_{K_2} channels is voltage and time dependent (Methods). The I_{K_2} activation parameter, s, is ~ 0 in steady state conditions at $V = -93$ mV, although the membrane potential does not remain near $V = -90$ mV sufficiently long, relative to τ_s, to enable s (dashed line in middle panel of Fig. 6 A) to reach its steady state value. The τ_s parameter with the

specific forms of α_s and β_s given in Eqs. 3 and 4 is a bell-shaped, instantaneous function of a potential having a maximum value of 1.2 s at $V = -79$ mV. At $V = -93$ mV, $\tau_s = 0.7$ s, at $V = -70$ mV, $\tau_s = 0.6$ s, and at $V = -60$ mV, $\tau_s = 0.2$ s. Consequently, τ_s rapidly increases from 0.6 s at the beginning of the simulation up to 1.2 s by $t = 155$ ms and then back down to 0.7 s at MDP (dashed line in middle panel of Fig. 6 A). The time needed for this initial hyperpolarization to MDP to take place (~ 10 ms) is significantly less than any of the values of τ_s, which the membrane scans as it moves from -70 to -93 mV. Therefore, s changes very little from its initial value ($s = 1$) throughout this phase, as illustrated by the dashed line in the top panel of Fig. 6 A. During pacemaker depolarization the membrane depolarizes from -93 to -60 mV in ~ 350 ms. Throughout the first part of this process, up until $t \simeq 375$ ms, the
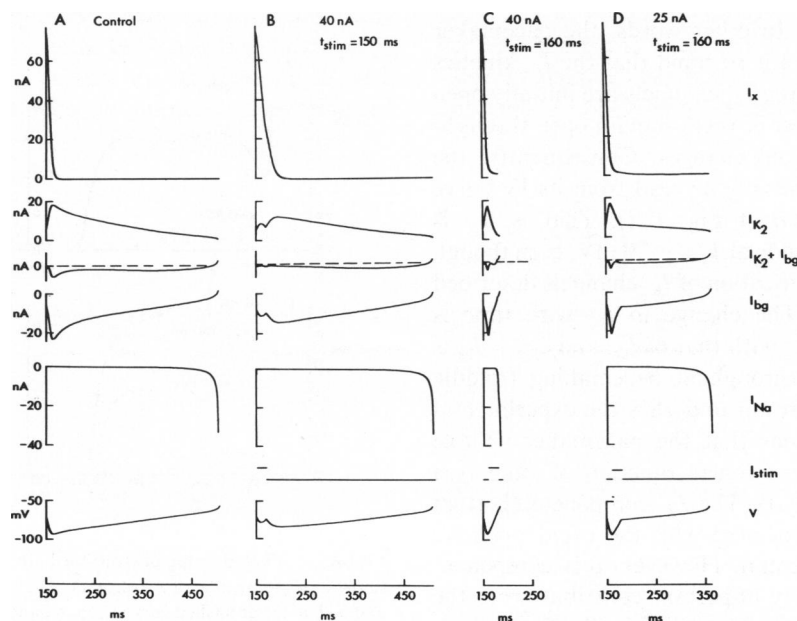

FIGURE 5 The time course of the currents I_x, I_{K_2}, I_{bg}, and I_{Na} during pacemaking (A), and phase resetting (B–D) in Model I, as described in the text. The two bottom panels represent the current pulse and the voltage changes during the pacemaker process.
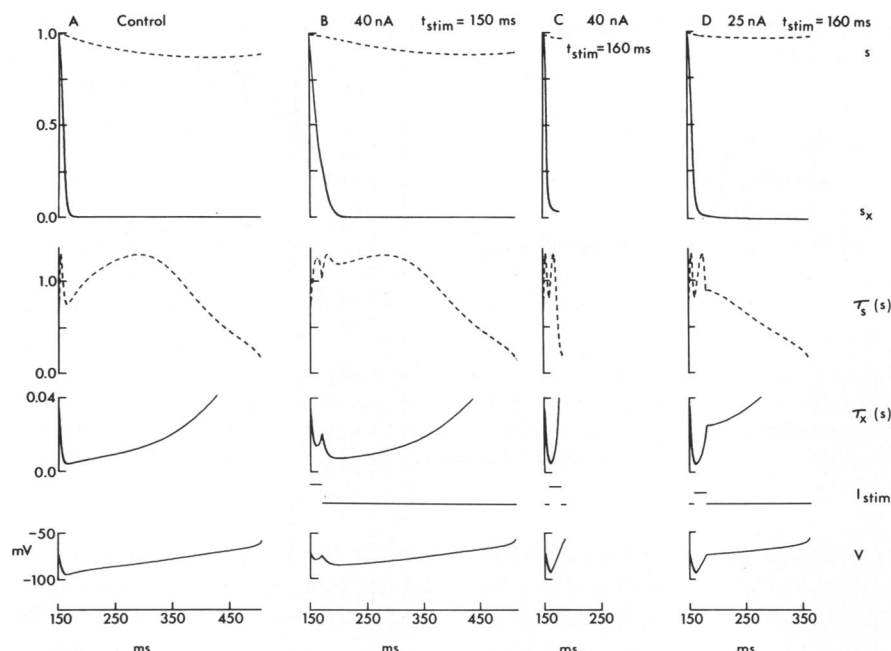
FIGURE 6   Time course of s, s_x, τ_s, and τ_x during pacemaking (A) and phase resetting (B–D) in Model I. The two bottom rows of panels represent the current stimulus and the pacemaker voltage changes.

potential lies in a range where s_∞ (the steady state value of s) is less than $s(t)$ (its instantaneous value). Consequently, s diminishes somewhat from its initial value. Throughout the latter part of pacemaking ($t > 375$ ms), s_∞ is greater than $s(t)$. Therefore, the $s(t)$ curve bends back up toward $s = 1$ (dashed line in top panel of Fig. 6 A). However, the duration of the pacemaker phase in Model I is significantly less than τ_s at almost all membrane potentials. Consequently, the overall change in s from its initial value is relatively small. Its minimum value is 0.86, which occurs at $\sim t \simeq 375$ ms. In other words, the pacemaker voltage change in Model I is so rapid that the I_{K_2} kinetics change very little. All of the I_{K_2} channels are initially open at $V = -70$ mV, and most of them remain open throughout the subsequent voltage changes. Consequently, the amplitude of I_{K_2} can essentially be read from its IV curve (given closely by curve a of Fig. 1 A). That is, I_{K_2} is relatively small in magnitude at $V = -70$ mV, even though $s = 1$, because of the rectification of I_{K_2} channels described by $f_{K_2}(V)$ (Methods). The change in I_{K_2} with time is roughly mirror symmetric with that of I_{bg}, and $I_{K_2} + I_{bg}$ is approximately constant throughout pacemaking (middle panel of Fig. 5 A). This result underlies the experimental and numerical observations that the pacemaker voltage change is approximately a linear function of time (see control tracings of Fig. 2 A). The I_{Na} component (bottom panel of Fig. 5 A) is associated with the rapid upstroke phase of the action potential. However, this component also makes an increasingly important contribution to the latter part of pacemaking, as illustrated by the $I_{Na}(t)$ curve of Fig. 5 A.

The analysis of this section is further illustrated by Fig.

7 A, which contains a part of the control trajectory of Fig. 4 A and B on an expanded ordinate scale together with the $I_{Na} + I_{K_2} + I_{bg}$ current-voltage relation with s set to its minimum value 0.86 at all potentials (dashed line). The initial phase of the trajectory from 0 to -4 nA is associated with the closing of I_x channels. The rest of the trajectory closely follows the $s = 0.86$ IV curve. The slight deviation of this curve from the $s = 0.86$ IV relation between -92 and -80 mV is due to the fact that s is slightly >0.86 during this part of the pacemaker process.
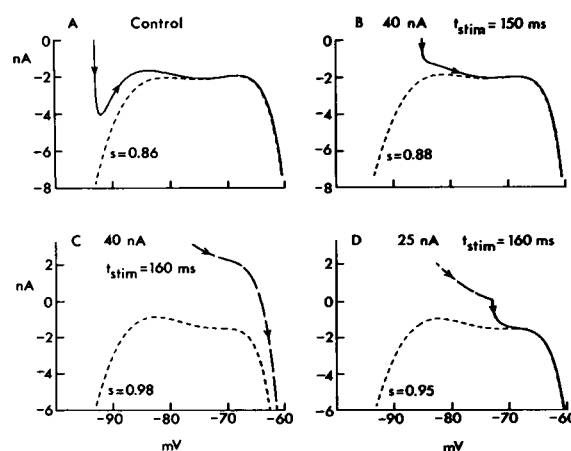

FIGURE 7   Relationship of trajectories in Model I to the IV appropriate to the minimum value of s for each of the simulation conditions in Figs. 5 and 6. The lower dashed curve in each panel correspond to $I_{bg} + I_{Na} + I_{K_2}$ with the s parameter set at the value shown throughout each simulation. The dashed portion of the trajectories in C and D occur during current-pulse injection.

Relationship of Phase Resetting to Ionic Currents in Model I

The time course of I_x, I_{K_2}, I_{bg}, and I_{Na} during phase resetting is illustrated in Figs. 5 B–D for a 40-nA pulse at t_{stim} = 150 ms, a 40-nA pulse at t_{stim} = 160 ms, and a 25-nA pulse at t_{stim} = 160 ms, respectively. The effect of the 40-nA pulse at t_{stim} = 150 ms is to counterbalance the outward current through the I_x channels. Consequently, during the initial phase of current injection the rate of hyperpolarization is reduced, since the I_x channels deactivate more slowly. The τ_x time course is illustrated in the middle panel of Fig. 6 B. This parameter increases during the latter part of the pulse because the membrane potential begins to depolarize during this time period (bottom panel of Fig. 6 B). However, by the end of the current injection at t = 170 ms, enough I_x channels are still open so that the net current is outward and the membrane once again begins to hyperpolarize. This hyperpolarizing phase is more gradual than in the control because of the increase in τ_x during and following the pulse (Figs. 6 A and B). Therefore, the overall effect of the pulse is to give a more rounded appearance to $V(t)$ near MDP. This result is evident in row B of Fig. 2 for both the experimental (t_{stim} = 130 ms) and the theoretical results (t_{stim} = 150 ms). The pulse also affects the balance between I_{K_2} and I_{bg} (Fig. 5 B). The depolarizing effect of the pulse causes the membrane potential to lie in a range where the magnitude of the sum of I_{K_2} and I_{bg} is smaller than in control. The magnitude of the slope of I_{bg} for $V \leq -90$ mV is greater than the slope of the fully activated I_{K_2} current-voltage relation for $V \leq -90$ mV (Fig. 1 A; curve d vs. curve a). In other words, the magnitude of $I_{K_2} + I_{bg}$ is greater at -90 mV than at -80 mV, as is apparent from curve b in Fig. 1 A. Since the membrane potential is depolarized by the pulse relative to control, the amplitude of $I_{K_2} + I_{bg}$ is reduced. The pulse also produces a subtle effect on the $s(t)$ curve (dashed line in the top panel of Fig. 6 B). Its depolarizing effect causes the membrane potential to lie in a range where τ_s is >1 s both during and after pulse application (Fig. 6 B). Consequently, the s parameter changes a little bit more slowly than it does in control, reaching a minimum value of 0.88 rather than 0.86. The sum of $I_{K_2} + I_{bg}$ is thereby reduced even further by this effect, which persists throughout almost the entire pacemaker phase. In other words, the current pulse effectively resets the slope of pacemaker depolarization to a smaller value through a combination of effects due to I_x, I_{K_2}, and I_{bg}. The t_{stim} = 150 ms results in row B of both the experimental and simulated records in Fig. 2 display this effect. Fig. 7 B again illustrates that the perturbed trajectory closely follows the IV curve appropriate for s =0.88 during the later part of diastolic depolarization.

The above analysis demonstrates that prolongation of IBI by a depolarizing pulse applied relatively early in the unperturbed cycle is produced by a slowing of I_x kinetics and by a decrease in the slope of pacemaker depolarization

due to changes in I_{K_2} and I_{bg}. However, both effects are offset to some extent by the depolarizing effect of the pulse itself, which activates I_{Na} more than in the control and tends to take the membrane to threshold more rapidly than in the control.

For a 40-nA stimulus injected at t_{stim} = 160 ms, or at later times, threshold is reached more rapidly than in the control. This is because the net hyperpolarizing current, carried by I_x, at $t_{stim} \geq 160$ ms is less than 40 nA. Consequently, throughout the entire duration of the pulse, there is a net depolarizing current given approximately by the difference between the instantaneous value of I_x and the injected stimulus of 40 nA. The result is a more rapid rate of membrane depolarization than in control and a significant reduction in IBI. The trajectory for these conditions with s = 0.98 is illustrated in Fig. 7 C. This value of 0.98 is the minimum value of s during the simulation simply because the time to threshold is very small in comparison to τ_s. The trajectory is shown as a dashed line to emphasize that the current pulse is being applied. The difference between the trajectory and the IV curve represents the contribution of I_x.

The effect of a depolarizing pulse on the time course of the currents at $t_{stim} \geq 160$ ms is less for a smaller pulse amplitude. This result is illustrated in Figs. 5 D and 6 D for a 25 nA pulse applied at t_{stim} = 160 ms. The analysis for these conditions is similar to that of Figs. 5 B and 6 B. The pulse slows I_x kinetics and it resets the $s(t)$ curve so that s reaches a minimum of 0.95. Nevertheless, IBI is reduced, because the depolarizing effect of the pulse brings the membrane to a potential that lies about halfway between MDP and threshold. Since I_{Na} is not significantly activated as a result of the pulse, the net effect is to shift $I_{K_2} + I_{bg}$ in the outward direction. Thus the membrane subsequently depolarizes to threshold more slowly than in the control. However, since there is a considerably smaller range of potential to cover in order to attain threshold, the IBI is reduced below the control value. The relationship of the trajectory to the IV appropriate for s = 0.95 is illustrated in Fig. 7 D.

The analysis of this section illustrates that a relatively large pulse would depolarize the membrane to threshold for t_{stim} = 150 ms were it not for I_x. Consequently, the transitional region between prolongation and shortening of IBI is shifted to earlier times in the cycle as pulse amplitude is increased. Moreover, the width of the transitional region is reduced for the larger pulses because threshold is reached earlier.

Phase Resetting of Model II

Experimental records of phase resetting from a preparation having an IBI_o >1 s are shown in the left-hand panel of Fig. 8. The diameter of this aggregate was 171 μm. Similar behavior was observed in two out of four preparations studied that had IBI_o >1 s. Model II is appropriate for
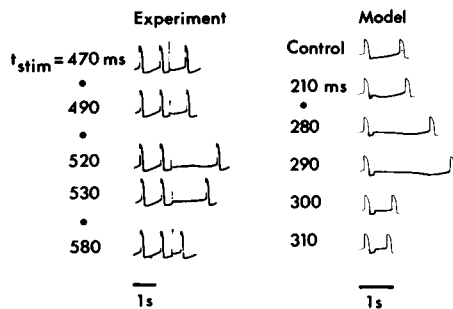
Experiment   Model

t_{stim} = 470 ms   Control

490   210 ms

                       280

520   290

530   300

580   310

1 s   1 s

FIGURE 8   Phase resetting of a preparation having an BI_0 >1 s. Left-hand panel: experimental records from an aggregate having a diameter of 171 μm and an IBI_0 of 1.1 s. MDP = -95 mV; maximum overshoot potential = +30 mV. A 20-ms duration pulse of 20-nA amplitude was applied at the times indicated. Right-hand panel: simulations of phase resetting of Model II by a 25-nA pulse injected at the times shown. These results were prepared in the same way as the model results in Fig. 2. The thicker solid lines beginning at -70 mV on the repolarization of the first action potential and ending at -55 mV on the rising phase of the second action potential correspond to the simulation results. The action potentials (thinner lines) are experimental traces grafted onto the simulation curves.

these somewhat slower beating preparations; it also has an IBI_0 >1 s, as shown by the control simulation in the right-hand panel of Fig. 8. Perturbation of both Model II and the corresponding experimental preparation revealed phase resetting characteristics that are similar to those of Model I for small pulses but that are fundamentally different from the results in Model I for larger pulse amplitudes. A 20-nA depolarizing pulse applied to the experimental preparation at t_{stim} = 490 ms and earlier produced slight prolongations of IBI comparable with those shown in Fig. 2 for a faster beating aggregate (IBI_0 ≃ 0.5 s). However, a much more substantial prolongation of IBI (IBI/IBI_0 ≃ 2.8) was observed when the pulse was applied at t_{stim} = 520 ms. This long prolongation was accompanied by a subthreshold oscillatory phase in the membrane potential before the succeeding action potential. A 20-nA pulse applied 10 ms later delayed the succeeding beat by approximately one and one-half cycles (IBI/IBI_0 ≃ 2.4). The membrane potential did not exhibit a subthreshold oscillation in this case. In the 19 faster beating preparations studied, subthreshold oscillatory activity was never observed. Phase resetting of Model II with a 25-nA pulse, shown in the right-hand panel of Fig. 8, qualitatively mimics most of the features in the experimental records. Specifically, the IBI is prolonged for stimulus times relatively early in the cycle; the action potential immediately following the pulse that produced maximum prolongation is preceded by a subthreshold oscillation; and there is an abrupt transition in IBI between t_{stim} = 290 and 300 ms. There are some discrepancies between theory and experiment, most notably in the relative temporal position in the cycle of this transitional region. Experimentally, the transition from prolongation to shortening of IBI occurs near the midpoint of the unperturbed cycle, about two or three action potential durations

removed from MDP. The transition in the model occurs ~30% into the cycle, approximately one action potential duration after MDP. This result is not an invariant prediction of our theoretical analysis. It depends to some extent upon the amplitude of the current pulse. Moreover, the transition point can be shifted to either earlier or later times in the cycle by modifying various model parameters, although our experience has suggested that it cannot be readily shifted very much beyond the 40% point, which would still be somewhat at odds with the preparation represented in Fig. 8. In any case, the model qualitatively mimics the voltage changes that occur subsequent to pulse injection.

Fig. 9 plots the phase-resetting curves for Model II in response to 15- and 25-nA pulses, with 1-ms increments in t_{stim}. The computed points for the 15-nA pulse merge together to give a continuous curve. The phase-resetting curve for the 25-nA pulse is apparently discontinuous. This is further illustrated by the phase plane analysis described in Fig. 10. The two points in Figs. 10 B-D represented by the symbol (●), and labeled V_1 and V_2, are the equilibrium points of the steady state current-voltage relation in the pacemaker voltage range (inset of Fig. 1 B). The trajectories in Fig. 10 A, B correspond to the unperturbed pacemaker and to the perturbations produced by a 15-nA current pulse applied at the times indicated on the Figures. These trajectories are qualitatively similar to those of Model I in Fig. 4. For example, the trajectory following a current pulse delivered at a given time lies to the right of a trajectory following a current pulse delivered at an earlier time. The 25-nA pulse trajectories in Figs. 10 C and D are fundamentally different in this respect. Fig. 10 C describes trajectories for a 25 nA pulse applied at t_{stim} = 0.23, 0.26, 0.28, or 0.296 s (solid lines) or at t_{stim} = 0.290, 0.293, 0.295 s (dotted lines). The trajectories during current pulse injection have been deleted from Fig. 10 C. The dotted lines in this case correspond to trajectories following

IBI/IBI_0
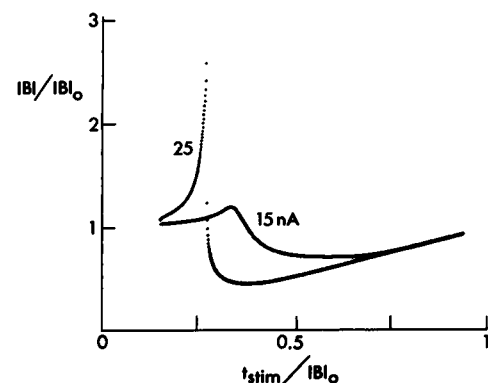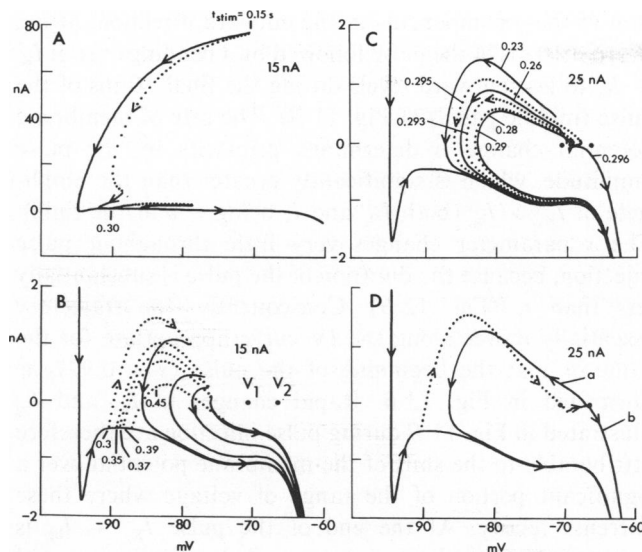
25

15 nA

0   0.5   1

t_{stim}/IBI_0

FIGURE 9   Normalized phase resetting curves for Model II with either a 15 or a 25-nA current pulse. The interval between each simulation was 1 ms. The results for the 15-ms pulse merge together to give a continuous curve. The results for 25 nA have an apparent discontinuity, as described in the text.

708

FIGURE 10 Current-voltage trajectories during phase resetting of Model II. (*A*) Unperturbed trajectory (outer curve) and perturbed trajectories for a 15-nA pulse applied at t_{stim} = 0.15 or 0.30 s. The dotted lines correspond to the trajectory during the 20-ms duration pulse. (*B*) Additional trajectories for a 15-nA pulse at the times indicated. Expanded current scale. The two symbols (●) represent the equilibrium points of Model II in the pacemaker voltage range at V_1 = −70.8 and V_2 = −66.7 mV (*inset* of Fig. 1 *B*). (*C*) Trajectories for a 25-nA pulse beginning at the times indicated. The trajectories during current injection are not shown in this panel. (*D*) Trajectories for a 25-nA pulse applied beginning at t_{stim} = 0.295501 s (curve *a*) and 0.295502 s (curve *b*). These two results essentially overlap during the time of injection of the current pulses (dotted line) and for a while immediately following the pulses, as they approach V_2. They subsequently diverge from this point.

current-pulse injection initiated at the times indicated. There is a change in the direction in which the trajectories in Model II move as t_{stim} is incremented for values of t_{stim} in the transitional region of the IBI vs. t_{stim} relation. The trajectories for t_{stim} = 0.23, 0.26, and 0.28 s have the same relationship to one another as do the trajectories in Fig. 10 *B*. However, the t_{stim} = 0.29 s trajectory lies to the left of the t_{stim} = 0.28 s trajectory, and the t_{stim} = 0.293 s and 0.295 s trajectories lie even farther to the left. The trajectories labeled *a* and *b* in Fig. 10 *D* correspond to t_{stim} = 0.295501 and 0.295502 s, respectively. The dotted line in Fig. 10 *D* is the trajectory for both *a* and *b* during current-pulse injection. The trajectories essentially overlap during this time, as well as during the time immediately following the pulse. The net current at the end of the pulse lies slightly in the inward direction. Therefore, the membrane slowly depolarizes and the trajectory slowly moves toward the unstable equilibrium point at $V = V_2$ = −66.7 mV. It then moves away from this point in either the inward direction eventually attaining threshold (curve *b*), or in the outward direction, away from threshold (curve *a*). Thus, the equilibrium point at V_2 appears to be a saddle point (FitzHugh, 1955; Jack et al., 1975). Both curves *a* and *b* ultimately rejoin the unperturbed cycle during the upstroke of the action potential. In the case of curve *a* the trajectory

effectively encloses a region of the IV phase plane containing the equilibrium point at $V = V_1$ = −70.8 mV before returning to the control trajectory. This equilibrium point also appears to be unstable, based on computer simulations with all activation and inactivation variables set equal to their steady state values appropriate to $V = V_1$ and V set equal to $V_1 \pm \Delta V$, where $\Delta V \le 0.1$ mV. The voltage moves away from V_1 under these conditions, exhibiting a pattern of oscillations of slowly increasing amplitude. Consequently, V_1 may be classified as an equilibrium point having the characteristics of an unstable spiral (Jack et al., 1975).

Curves *a* and *b* in Fig. 10 *D* closely approximate the trajectories that occur after the phase point has remained near V_2 for an arbitrarily long time. This result can be demonstrated by setting all of the variables of Model II at their appropriate steady state values corresponding to $V = V_2$ and by setting $V = V_2 \pm \Delta V$ with $\Delta V \le 0.1$ mV. The resulting trajectory for the $V = V_2 - \Delta V$ initial condition is within a line width of curve *a* except near $V = −80$ mV, where the difference in current between the two trajectories is ~0.1 nA. The trajectory for the $V = V_2 + \Delta V$ initial condition is virtually indistinguishable from curve *b*. The time difference that the phase point takes to move along these two trajectories is ~1.32 s. That is, the IBI vs. t_{stim} relation is discontinuous in the sense that the phase point must move away from V_2 in either the hyper- or depolarizing direction no matter how long it remains near V_2. The maximum value of IBI is unbounded, because the nearer the phase point approaches V_2 the longer it subsequently remains near V_2, where $\dot{V}$ is very small (FitzHugh, 1955). Consequently, the IBI vs. t_{stim} relation has a singularity in the critical region for a 25-nA pulse amplitude.

Relationship of Phase Resetting to Ionic Currents in Model II

The contributions of I_x, I_{bg}, I_{K_2}, and I_{Na} to spontaneous pacemaking in Model II are shown in Fig. 11 *A*. These results are qualitatively similar to those of Model I. The I_x component underlies the initial hyperpolarizing phase, the I_{K_2} and I_{bg} components underlie most of the pacemaker phase, and I_{Na} contributes to the latter phase of pacemaking before full activation of I_{Na}. The primary quantitative difference is in the slope of pacemaking which is smaller in Model II than in Model I. This difference results in a slower diastolic depolarization that permits a greater overall change in the *s* variable (top panel, Fig. 12 *A*), which reaches a minimum value of 0.60, as compared with 0.86 in Model I. The control trajectory and the IV for *s* = 0.60 are both shown in Fig. 13 *A*.

The differences in the models are attributable to the fact that I_{bg} in Model II is essentially shifted upward along the current axis by a small amount (curves *d* in Figs. 1 *A* and *B*). A further consequence of this result is that the sum of I_{bg} and the fully activated I_{K_2} component lies in the
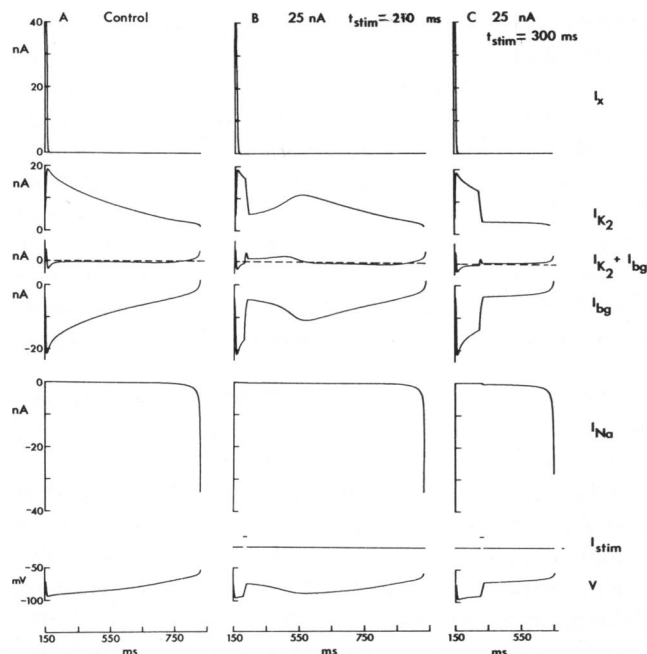
FIGURE 11 The time course of the currents I_x, I_{K_2}, I_{bg}, and I_{Na} during pacemaking (A) and phase resetting (B–C) in Model II, as described in the text. The two bottom panels represent the current stimulus and pacemaker voltage changes.

outward current direction for $-90 \leq V \leq -65$ mV (curve b, Fig. 1 B). Thus, the sum $I_{K_2} + I_{bg}$ contributes to the repolarization of the action potential (Fig. 11 A). From about the time that MDP is attained, the sum $I_{K_2} + I_{bg}$ becomes inward and s slightly deactivates, which causes $I_{K_2} + I_{bg}$ to lie further inward. A depolarizing pulse can force $I_{K_2} + I_{bg}$ to be outward once again, thereby producing prolongation of IBI. This result is illustrated by Figs. 11 B, 12 B, and 13 B for a 25 nA pulse delivered at $t_{stim} = 210$ ms. The effect of the pulse on I_{bg} and I_{K_2} is to rapidly move the

sum of these components in the outward direction during the first 10 ms of the pulse followed by a bending over of $I_{K_2} + I_{bg}$ to less outward levels during the final 10 ms of the pulse (middle panels of Fig. 11 B). The rate of membrane potential change is determined primarily by the pulse amplitude, which is significantly greater than the amplitude of $I_{K_2} + I_{bg}$ (both I_{Na} and I_x being $\simeq 0$ at the time). The s parameter changes very little throughout pulse injection, because the duration of the pulse is substantially less than τ_s (Fig. 12 B). Consequently, the trajectory essentially moves along the IV curve appropriate for the value of s at the beginning of the pulse (s = 0.92), as illustrated in Fig. 13 B. Rapid changes in I_{K_2} and I_{bg} illustrated in Fig. 11 B during pulse injection are therefore attributable to the shift of the membrane potential over a significant portion of the range of voltage where these currents rectify. At the end of the pulse $I_{K_2} + I_{bg}$ is outward. The membrane subsequently hyperpolarizes, and the trajectory deviates downward from the s = 0.92 IV curve as s resumes its deactivation time course. The sum of I_{K_2} and I_{bg} eventually becomes inward once again and pacemaker depolarization resumes in a manner similar to that of the control simulation (bottom panels of Figs. 11 A and B). The delay in resumption of pacemaking can be a significant fraction of the duration of the unperturbed cycle, because the hyperpolarizing phase is controlled by the I_{K_2} kinetics and $\tau_s \sim 1$ s (Fig. 12 B). The effect of the pulse is to rapidly move τ_s from 0.7 at $V \simeq -90$ mV on the ascending limb of the bell-shaped τ_s vs. V curve to its maximum value at $V = -79$ mV, and then to $\tau_s = 0.75$ on the descending limb of the bell-shaped curve. The membrane then slowly hyperpolarizes, with τ_s moving toward the maximum τ_s. Consequently, the rate of hyperpolarization is slower than the rate of pacemaker depolarization in the control simulation, because the average τ_s value during this hyperpolarizing phase is greater than the average τ_s
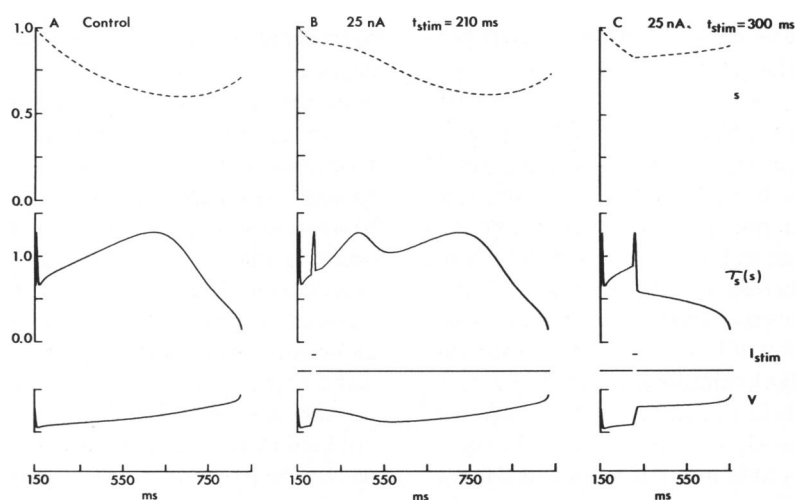

FIGURE 12 Relationship of s and τ_s to pacemaking and phase resetting in Model II. The two bottom panels represent the current stimulus and the pacemaker voltage changes.
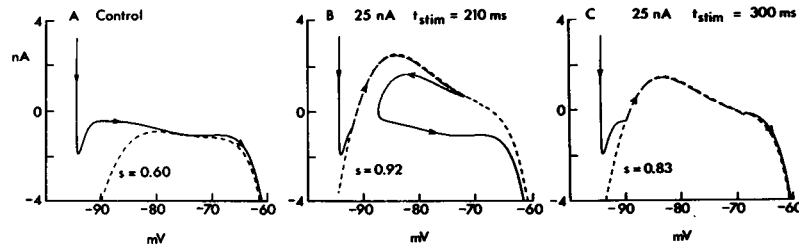
FIGURE 13   Relationship of trajectories in Model II to IV curves for the simulation conditions of Figs. 11 and 12. Panel A illustrates the control trajectory with the $I_{K_2} + I_{bg} + I_{Na}$ curve with $s = 0.60$ throughout, which is the minimum value of s during the simulation. Panel B illustrates the trajectory for a 25-nA pulse applied at $t_{stim} = 210$ ms together with the IV appropriate for $s = 0.93$, which is the value of s at the beginning of the pulse. The trajectory (———) and the IV curve (---) essentially overlap throughout the duration of the pulse. Panel C illustrates the trajectory for a 25-nA pulse applied at $t_{stim} = 300$ ms together with the IV curve for $s = 0.83$, which is the value of s at the beginning of pulse injection.

value during the depolarization to threshold. In this way IBI is prolonged. Considerably greater prolongation can be achieved when the net current at the end of the pulse is $\simeq 0$ and the s variable at the beginning of the pulse is approximately the same as its value at $V = V_2$. Under these conditions the phase point will move very slowly toward the V_2 saddle point before moving away from it in either the hyper- or depolarizing direction as described above.

A significant reduction of IBI will be produced by a pulse that depolarizes the membrane into the region where I_{Na} is activated. This result is illustrated by a 25-nA pulse applied at $t_{stim} = 300$ ms (Figs. 11 C, 12 C, 13 C). The trajectory follows the IV curve appropriate for the s value at 300 ms ($s = 0.83$) during pulse injection (Fig. 13 C). Near the end of this pulse I_{Na} is partially activated so that the net current ($I_{K_2} + I_{bg} + I_{Na} + I_x$) at 320 ms is inward (Fig. 11 C). The current-voltage phase point is sufficiently far from $V = V_2$ so that the membrane potential does not linger very long near the saddle point. The s parameter is reset by the pulse in a manner similar to that of Model I so that the slope of depolarization following the pulse is reduced compared with the control. However, the membrane potential is already close to threshold. Only a small additional depolarization is required before I_{Na} is fully activated. Consequently, IBI is reduced.

The above analysis demonstrates the relationship between pulse amplitude and the transitional region of the IBI vs. t_{stim} relation. The rate of membrane depolarization throughout pulse injection in Model II is determined primarily by the pulse amplitude itself even for pulses as small as a few nA, because $I_{K_2} + I_{bg}$ is only $\simeq -1$ nA during pacemaker depolarization and I_x is negligible. Prolongation in Model II is produced when a current pulse resets $I_{K_2} + I_{bg}$ to an outward level. This process can only occur relatively early in the cycle when $s \simeq 1$.

DISCUSSION

Injection of a current pulse of brief duration into an aggregate of electrically coupled, spontaneously beating heart cells produces a transient change in the beat frequency of the preparation. The time of occurrence of the first beat following current-pulse injection is modified to an extent that depends upon the amplitude of the pulse and the time in the unperturbed cycle at which it is applied. The aggregate resumes its normal spontaneous activity usually within one cycle after stimulation (Fig. 2). Consequently, the effect of the pulse is to shift, or reset the phase of spontaneous activity. Phase resetting is clearly a continuous function of the time of pulse injection for relatively small amplitude pulses. Experimentally, phase resetting appears to be a discontinuous function of the time of pulse injection for larger pulse amplitudes.

Our modeling results are summarized in Fig. 14, which schematically illustrates the limit cycle trajectories in the IV phase plane, the steady state IV curve, and the IBI vs. t_{stim} results for Models I and II. The limit cycle of Model I encloses one equilibrium point in the IV phase plane, whereas the Model II limit cycle encloses three equilibrium points. This difference is produced essentially by a shift of the IV curve along the membrane current axis. Both models exhibit Type I phase resetting (Winfree, 1977, 1980) for small pulse amplitudes, as illustrated by curve a in the lower panels of Fig. 14. A larger pulse amplitude in Model I produces phase resetting that is a very steep function of t_{stim}. In fact, IBI appears to be a discontinuous function of t_{stim} when 0.5 ms time increments are used. However, an analysis of phase resetting on a much finer time scale (10-μs increment in t_{stim}) reveals that the IBI vs. t_{stim} relation is fundamentally continuous (curve b for Model I, lower panel of Fig. 14). The apparent discontinuity of Model I that we have described is associated with the properties of I_{Na}. The I_{Na} component has a steep voltage dependence near $V = -60$ mV. In fact, it confers an apparent discontinuity to excitable membranes referred to as an all-or-none threshold. However, detailed modeling and experimental examination of I_{Na} in nerve, which is similar to I_{Na} in heart, has revealed that the voltage attained at the end of a pulse is fundamentally a continuous function of stimulus strength (FitzHugh, 1955; Cole et al., 1970; Clay, 1977). Our analysis of Model I thus reveals similar behavior in a cardiac model. Furthermore, numerical studies of the Hodgkin-Huxley equations suggest that
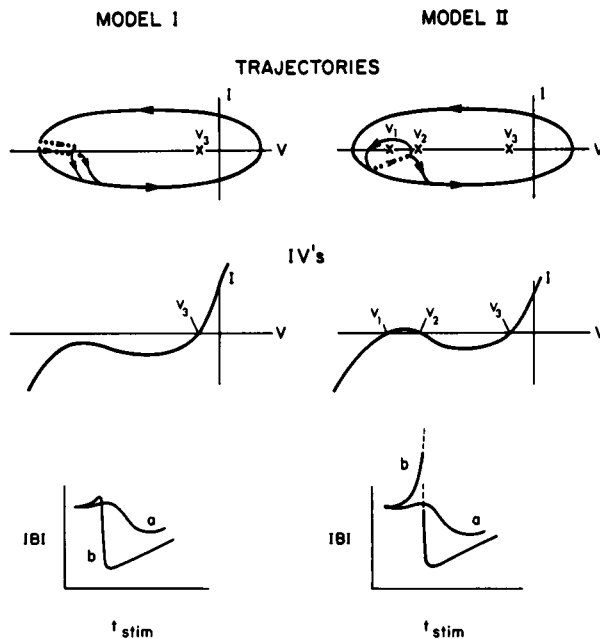
MODEL I   MODEL II

FIGURE 14 Schematic illustration of the phase resetting analysis of Models I and II. The ellipsoidal curves in the top panel represent the limit cycle trajectories in the IV phase plane together with the equilibrium points (●) of the respective IV curves (middle panel) and the results of current pulse perturbations near the critical region of the $IBI-t_{stim}$ relation (curve b for Model I and for Model II, lower panel). Model I has one equilibrium point, whereas Model II has three equilibrium points. The IBI vs. t_{stim} relation in Model I is fundamentally continuous both for small (curve a) and large (curve b) pulse amplitudes. Model II exhibits similar behavior, although the IBI vs. t_{stim} relation is singular (curve b) for some pulse amplitudes, as described in the text.

phase-resetting can be very steeply changing but fundamentally continuous (Best, 1979). Since both levels of stimulus intensity used in Model I lead to Type 1 phase resetting, we therefore caution against inferal of Type 0 phase-resetting simply based upon the existence of an apparent discontinuity in experimentally obtained plots of IBI vs. t_{stim} (Scott, 1979; Winfree, 1980; Winfree, 1981).

Model II also exhibits Type 1 phase resetting for sufficiently low stimulus intensities (curve a for Model II, lower panel of Fig. 14). For greater pulse amplitudes (≈ 25 nA), illustrated by curve b, the state point is perturbed near the saddle point at V_2 over a certain range of coupling intervals. For one value of t_{stim} the separatrix of the saddle point is presumably encountered, IBI becomes unbounded, and spontaneous oscillation ceases. In this case a topological degree cannot be assigned to the phase resetting. However, the membrane potential will not rest indefinitely at a saddle equilibrium point in the presence of noise, because an equilibrium point of this type is unstable. Moreover, the equilibrium point at $V = V_1$ in Model II is also unstable. Consequently, experimental preparations that are described by our Model II analysis cannot be made quiescent with a resting potential in the pacemaker voltage range by injection of a current pulse of brief

duration. A further shift of the IV in the outward direction may produce a system with a stable equilibrium point at V_1, which is capable of generating spontaneous activity. However, we have not explored this additional modification of our model. Spontaneous activity can be annihilated by a single pulse in nerve and in other cardiac preparations that have a stable equilibrium point (Best, 1979; Guttman et al., 1980; Jalife and Antzelevitch, 1979; 1980).

Our results illustrate a general difference between nerve and cardiac cells. Cardiac cells usually exhibit an N-shaped steady state IV with a region of negative slope conductance, whereas nerve cells generally have a monotonic steady state IV with a positive slope conductance for all membrane potentials (Jack et al., 1975). The underlying cause of this difference can be explained by a comparison of the potassium current, I_K, in these different cell types. I_K in heart is relatively small in comparison with I_K in nerve, and it displays inward rectification with negative slope conductance. I_K in nerve has a positive slope IV. Consequently, I_K in nerve does not contribute a negative slope character to the total IV, and its relatively large amplitude effectively masks the negative slope character of I_{Na} in steady state conditions. Therefore, the total IV has only a single equilibrium point regardless of its absolute position on the current-voltage axes. For example, the Hodgkin and Huxley (1952) model of squid axon can be made repetitive either by the addition of a small bias current to the model or by a shift in the gating parameters appropriate to a slight reduction of the external calcium ion concentration (Huxley, 1959). The IV curve underlying this behavior is monotonic with a single equilibrium point at $V = -55$ mV. An exception to this model for nerve cells is provided by the R15 pacemaker cell in *Aplysia*, which exhibits an N-shaped IV under some experimental conditions (Adams et al., 1980)

Our analysis is also relevant for other cardiac preparations, especially cardiac Purkinje fibers, which have many properties in common with ventricular cells from 7–d–old chick embryonic hearts (Clay and Shrier, 1981a). In particular, the McAllister et al. (1975) model of cardiac Purkinje fiber pacemaker activity has an N-shaped steady state IV with negative slope conductance and a single equilibrium point, similar to our Model I. However, their IV curve with $s = 1$ lies above the voltage axis for $-90 \leq V \leq -65$ mV (Fig. 3 of McAllister et al., 1975), whereas the corresponding IV curve in our Model I lies below the voltage axis for all potentials in the pacemaker range (curve b of Fig. 1 A). Consequently, their model is intermediate to our Models I and II, although it can be made to correspond more closely to either Model I or II by relatively small shifts of the IV curve along the membrane current axis. The ionic mechanisms underlying phase resetting in the McAllister et al. (1975) model would differ from our analysis if the DiFrancesco (1981) reinterpretation of the pacemaker currents in Purkinje fibers is correct. The sign of the time-dependent pacemaker current would

be changed, and the background current would be modified, primarily by the removal of most, or all, of the background sodium conductance (DiFrancesco, 1981; DiFrancesco and Noble, 1982b). The negative slope features in the model would be contained entirely in I_{K_2} and I_{Na}. Nevertheless, the basic elements of phase resetting phenomena would be unchanged (DiFrancesco, 1981; DiFrancesco and Noble, 1982a). The essential ingredients for Purkinje fibers are time-dependent pacemaker current, a negative slope character in either a background or a time-dependent pacemaker current, the I_{Na} current, and an N-shaped steady state IV which can lead to either one, two, or three equilibrium points.

Our analysis is also relevant for embryonic atrial cell aggregates. These preparations do not exhibit time-dependent current kinetics in the pacemaker voltage range (Shrier and Clay, 1982). Nevertheless, they beat spontaneously and rhythmically with an IBI_0 of $\simeq 1$ s (Sachs and DeHaan, 1973; Shrier and Clay, 1982). The mechanisms that underly this activity are I_x, I_{Na}, and I_{bg}. The I_{bg} component differs considerably from I_{bg} in ventricular cell preparations in that it has a high slope resistance throughout the entire pacemaker voltage range and displays a smaller degree of inward rectification. These properties together with those of I_{Na} can produce an IBI_0 of 1 s or longer (Shrier and Clay, 1982). This system is spontaneously active only if its IV has one equilibrium point that lies positive to the threshold of I_{Na}. Spontaneous activity will not occur if the IV is shifted in the outward direction so that the equilibrium point lies below threshold. Hence, the phase resetting properties of this system are expected to be similar to those of Model I.

Our study demonstrates that the ionic current mechanisms that underlie phase resetting properties of embryonic cardiac cells are complex. Current pulses introduced during and immediately after repolarization reset the interbeat interval primarily by influencing the outward current, I_x. Greater prolongations in the interbeat interval resulting from current pulses at later times in the cycle are largely attributed to the predominating influence of changes in the pacemaker current, I_{K_2}. Finally, shortening of the interval is attributed ultimately to a premature activation of the rapid inward current, I_{Na}. A more complete ionic model of electrical activity of embryonic ventricular heart cell aggregates or modifications to the existing pacemaker model may remove some of the discrepancies between experiment and the presently existing partial model.

REFERENCES

Adams, W. B., I. Parnas, and I. B. Levitan. 1980. Mechanism of long lasting synaptic inhibition in *Aplysia* neuron R15. *J. Neurophysiol. (Bethesda).* 44:1148–1160.

Attwell, D., I. Cohen, D. Eisner, M. Ohba, and C. Ojeda. 1979. The steady state TTX-sensitive ("window") sodium current in cardiac Purkinje fibers. *Pfluegers Arch. Eur. J. Physiol.* 379:137–142.

Ayers, J. L., and A. I. Selverston. 1977. Synaptic control of an endogenous pacemaker network. *J. Physiol. (Paris).* 73:453–461.

Best, E. N. 1979. Null space in the Hodgkin-Huxley equations. A critical test. *Biophys. J.* 27:87–104.

Bristow, D. G., and J. W. Clark. 1982. A mathematical model of primary pacemaking cell in 5A node of the heart. *Am. J. Physiol.* 243:H207–H218.

Clapham, D. E. 1979. A whole tissue model of heart cell aggregates: electrical coupling between cells, membrane impedance, and the extracellular space. Ph.D. dissertation, Emory University, Altanta, GA.

Clay, J. R. 1977. Monte Carlo simulation of membrane noise: an analysis of fluctuations in graded excitation of nerve membrane. *J. Theor. Biol.* 64:671–680.

Clay, J. R., and M. F. Shlesinger. 1977. Random walk analysis of potassium fluxes associated with nerve impulses. *Proc. Natl. Acad. Sci. USA.* 74:5543–5546.

Clay, J. R., and M. F. Shlesinger. 1983. Effects of external cesium and rubidium on outward potassium currents in squid axons. *Biophys. J.* 42:43–53.

Clay, J. R., L. J. DeFelice, and R. L. DeHaan. 1979. Current noise parameters derived from voltage noise and impedance in embryonic heart cell aggregates. *Biophys. J.* 28:169–184.

Clay, J. R., and A. Shrier. 1981a. Analysis of subthreshold pace-maker currents in chick embryonic heart cells. *J. Physiol. (Lond.).* 312:471–490.

Clay, J. R., and A. Shrier. 1981b. Developmental changes in subthreshold pace-maker currents in chick embryonic heart cells. *J. Physiol. (Lond.).* 312:491–504.

Clay, J. R., and A. Shrier. 1983. Further evidence that I_{K_2} in chick embryonic heart cells is a potassium ion current. *Biophys. J.* 41(2, Pt. 2):312a. (Abstr.)

Cole, K. S., R. Guttman, and F. Bezanilla. 1970. Nerve membrane excitation without threshold. *Proc. Natl. Acad. Sci. USA.* 65:884–891.

Colizza, D., M. R. Guevara, and A. Shrier. 1983. A comparative study of collagenase- and trypsin-dissociated embryonic heart cells: reaggregation, electrophysiology, and pharmacology. *Can. J. Physiol. Pharmacol.* 61:408–419.

DeFelice, L. J., and R. L. DeHaan. 1977. Membrane noise and intercellular communication. *Proc. IEEE (Inst. Electr. Electron. Eng.) (Spec. Issue Biol. Signals).* 65:796–799.

DeHaan, R. L., and H. A. Fozzard. 1975. Membrane response to current pulses in spheroidal aggregates of embryonic heart cells. *J. Gen. Physiol.* 65:207–222.

DiFrancesco, D. 1981. A new interpretation of the pace-maker current in calf Purkinje fibers. *J. Physiol. (Lond.).* 314:359–376.

DiFrancesco, D., and D. Noble. 1982a. Implications of the re-interpretation of i_{K_2} for the modelling of the electrical activity of pacemaker tissues in the heart. *In* Cardiac Rate and Rhythm. L. N. Bouman and H. J. Jongsma, editors. Martinus Nijhoff Publishers. The Hague, Netherlands. 93–128.

DiFrancesco, D., and D. Noble. 1982b. Reconstruction of voltage-clamp currents in spherical cell aggregates from cardiac muscle. *J. Physiol. (Lond.).* 326:65–66P.

Ebihara, L., and E. A. Johnson. 1980. Fast sodium current in cardiac muscle. A quantitative description. *Biophys. J.* 32:779–790.

Ebihara, L., N. Shigeto, M. Lieberman, and E. A. Johnson. 1980. The

initial inward current in spherical clusters of chick embryonic heart cells. *J. Gen. Physiol.* 75:437–456.

FitzHugh, R. 1955. Mathematical models of threshold phenomena in the nerve membrane. *Bull. Math. Biophys.* 17:257–278.

Guevara, M. R., L. Glass, and A. Shrier. 1981. Phase locking, period-doubling bifurcations, and irregular dynamics in periodically stimulated cardiac cells. *Science (Wash. DC).* 214:1350–1353.

Guevara, M. R., and L. Glass. 1982. Phase locking, period doubling bifurcations and chaos in a mathematical model of a periodically driven oscillator: a theory for the entrainment of biological oscillators and the generation of cardiac dysrhythmias. *J. Math. Biol.* 14:1–23.

Guevara, M. R., L. Glass, M. C. Mackey, and A. Shrier. 1983. Chaos in neurobiology. *IEEE (Inst. Electr. Electron. Eng.) Trans. Systems, Man, and Cybernetics.* 13(5):790–798.

Guevara, M. R., A. Shrier, J. R. Clay, and L. Glass. 1982. Perturbation of spontaneous activity of embryonic chick heart cell aggregates by brief duration current pulses. *Biophys. J.* 37(2, Pt. 2):244a. (Abstr.)

Guttman, R., S. Lewis, and J. Rinzel. 1980. Control of repetitive firing in squid axon membrane as a model for a neuroneoscillator. *J. Physiol. (Lond.).* 305:377–395.

Hartline, D. K. 1976. Simulation of phase-dependent pattern changes to perturbations of regular firing in crayfish stretch receptor. *Brain Res.* 110:245–257.

Hodgkin, A. L., and A. F. Huxley. 1952. A quantitative description of membrane current and its application to conduction and excitation in nerve. *J. Physiol. (Lond.).* 117:500–544.

Huxley, A. F. 1959. Ion movements during nerve activity. *Ann. NY Acad. Sci.* 81:221–246.

Jack, J. J. B., D. Noble, and R. W. Tsien. 1975. Electric Current Flow in Excitable Cells. Clarendon Press, Oxford.

Jalife, J., and C. Antzelevitch. 1979. Phase resetting and annihilation of pacemaker activity in cardiac tissue. *Science (Wash. DC).* 206:695–697.

Jalife, J., and C. Antzelevitch. 1980. Pacemaker annihilation: diagnostic and therapeutic implications. *Am. Heart J.* 100:128–130.

Jalife, J., and G. K. Moe. 1976. Effect of electrotonic potentials on pacemaker activity of canine Purkinje fibers in relation to parasystole. *Circ. Res.* 39:801–808.

Jalife, J., A. J. Hamilton, V. R. Lamanna, and G. K. Moe. 1980. Effects of current flow on pacemaker activity of the isolated kitten sinoatrial node. *Am. J. Physiol.* 238:H307–H316.

Josephson, I., and N. Sperelakis. 1982. On the ionic mechanism underlying adrenergic-cholinergic antagonism in ventricular muscle. *J. Gen. Physiol.* 79:69–86.

Katz, B. 1949. Les constantes electriques de la membrane du muscle. *Arch. Sci. Physiol.* 3:285–299.

Mathias, R. T., L. Ebihara, M. Lieberman, and E. A. Johnson. 1981. Linear electrical properties of passive and active currents in spherical heart cell clusters. *Biophys. J.* 36:221–242.

McAllister, R. E., D. Noble, and R. W. Tsien. 1975. Reconstruction of the electrical activity of cardiac Purkinje fibres. *J. Physiol. (Lond.).* 251:1–59.

Nathan, R. D., and R. L. DeHaan. 1979. Voltage clamp analysis of embryonic heart cell aggregates. *J. Gen. Physiol.* 73:175–198.

Noble, D., and R. W. Tsien. 1968. The kinetics and rectifier properties of the slow potassium current in cardiac Purkinje fibres. *J. Physiol. (Lond.).* 195:185–214.

Perkel, D. J., J. H. Schulman, T. H. Bullock, G. P. Moore, and J. P. Segundo. 1964. Pacemaker neurons: effects of regularly spaced synaptic input. *Science (Wash. DC).* 145:61–63.

Pinsker, H. M. 1977. *Aplysia* bursting neurons as endogenous oscillators. I. Phase response curves for pulsed inhibitory synaptic input. *J. Neurophysiol. (Bethesda).* 40:527–543.

Rush, S., and H. Larsen. 1978. A practical algorithm for solving dynamic membrane equations. *IEEE (Inst. Electr. Electron. Eng.) Trans. Biomed. Eng.* 25:389–392.

Sachs, H. G., and R. L. DeHaan. 1973. Embryonic myocardial cell aggregates: volume and pulsation rate. *Dev. Biol.* 30:233–240.

Sano, T., T. Sawanobori, and H. Adaniya. 1978. Mechanism of rhythm determination among pacemaker cells of the mammalian sinus node. *Am. J. Physiol.* 235:H379–H384.

Scott, S. W. 1979. Stimulation simulations of young yet cultured beating hearts. Ph.D. Dissertation, State University of New York at Buffalo, Buffalo, NY.

Shrier, A., and J. R. Clay. 1980. Pacemaker currents in chick embryonic heart cells change with development. *Nature (Lond.).* 283:670–671.

Shrier, A., and J. R. Clay. 1982. Comparison of the pacemaker properties of chick embryonic atrial and ventricular heart cells. *J. Membr. Biol.* 69:49–56.

Ushiyama, J., and C. McC. Brooks. 1974. Intracellular stimulation and recording from single cardiac cells in the rabbit atrium. *J. Electrocardiol. (San Diego).* 7:119–126.

Weidmann, S. 1951. Effect of current flow on the membrane potential of cardiac muscle. *J. Physiol. (Lond.).* 115:227–236.

Winfree, A. T. 1977. Phase control of neural pacemakers. *Science (Wash. DC).* 197:761–763.

Winfree, A. T. 1980. The Geometry of Biological Time. Springer-Verlag, New York.

Winfree, A. T. 1981. Pecularities in the impulse response of pacemaker neurons. *In* Mathematical Aspects of Physiology. F. C. Hoppensteadt, editor. American Mathematical Society, Providence. 265–279.

Ypey, D., W. P. M. van Meerwijk, and R. L. DeHaan. 1982. Synchronization of cardiac pacemaker cells by electrical coupling. A study with embryonic heart cell aggregates and pacemaker cell models. *In* Cardiac Rate and Rhythm. L. N. Bouman and H. J. Jongsma, editors. Martinus Nijhoff Publishers. The Hague, Netherlands. 363–395.